Desalination and Water Treatment
www.deswater.com

doi: 10.1080/19443994.2014.928237

55 (2015) 1922–1933
August

Taylor & Francis
Taylor & Francis Group

Application of artificial neural network (ANN) for modeling of dyes decolorization by Sn/Zn-TiO_2 nanoparticles

Robab Mohammadi[a,*], Hamed Eskandarloo[b], Mohammad Mohammadi[c]

[a]*Department of Chemistry, Payame Noor University, P.O. Box 19395-3697, Tehran, Iran, Tel. +98 411 5421414; Fax: +98 411 5431067; email: mohammadi_rb@yahoo.com*
[b]*School of Chemistry, College of Science, University of Tehran, Tehran, Iran, Tel. +98 21 22235314; Fax: +98 21 22235114; email: eskandarloo@ut.ac.ir*
[c]*Faculty of Engineering, Mechanical Engineering Department, Urmia University, Urmia, Iran, Tel. +98 441 2813202; Fax: +98 441 4761165; email: m.mohammadi67@gmail.com*

Received 2 January 2014; Accepted 21 May 2014

This study examined the implementation of artificial neural network (ANN) for the prediction and modeling of methylene blue (MB) and methyl orange (MO) dyes decolorization in aqueous solution using Sn/Zn-TiO_2 nanoparticles prepared by sol–gel method. Operational parameters such as amount of catalyst, concentration of dye, reaction time, and temperature of solution were employed as inputs to the network and dye decolorization efficiency was the output of the network. ANN predicted results are in good agreement with the experimental results data with a correlation coefficient (R^2) of 0.9839 and 0.9887 for MB and MO dyes, respectively. The sensitivity analysis investigated that studied parameters have different effect on dyes decolorization. For both dyes, reaction time is the most influential parameter and the temperature of solution is the less influential variable in the removal efficiency of both dyes. The results indicated that neural network modeling could effectively predict and model the photocatalytic activity of the prepared Sn/Zn-TiO_2 nanoparticles.

Keywords: Sn/Zn-TiO_2 nanoparticles; Sol–gel method; Photocatalytic activity; Operational parameters; Artificial neural network

1. Introduction

Large quantities of dyes are produced and used in various industries including textile, cosmetic, paper, leather, pharmaceutical and nutrition industries [1]. The presence of dyes even at very low concentrations in effluent is highly visible and undesirable. It causes some serious problems to aquatic life and human health [2]. Diverse methods such as precipitation, adsorption, air stripping, flocculation, reverse osmosis, and ultrafiltration have been used for pollutant removal from aqueous solution. However, these processes only transfer organic pollutants from liquid to solid phase, giving rise to new type of pollution and requiring further treatment [3–6]. In recent years, advanced oxidation processes (AOPs) have been used for complete decolorization of organic pollutants [7]. Heterogeneous photocatalysis as one of the AOPs can provide an interesting route to complete destruction of contaminants to CO_2, H_2O, and corresponding mineral acids [8]. Among various semiconductors, much consideration has been given to TiO_2 due to its outstanding chemical stability, nontoxicity, low cost, and excellent destruction of organic contaminants [9].

*Corresponding author.

However, photocatalytic efficiency is low due to fast recombination of photogenerated electron–hole pairs [10]. Doping of a metal ion in a semiconductor is known to improve the trapping of electrons and inhibit electron–hole recombination [11]. There are many reports in the case of doping single metal ion which can enhance the photocatalytic efficiency of TiO_2. However, there are only a few papers concerning with codoping both metal ions for nanosized TiO_2 [12].

Intrinsic and extrinsic factors can influence decolorization of pollutant. The factors such as crystallinity, surface area, morphology, and optical absorption are related to intrinsic factors. Extrinsic factors are related to the operational parameters such as pollutant concentration, photocatalyst loading, intensity and wavelength of UV light, temperature, and reaction time. Also, the destruction rate can be affected by the presence of oxidants, dissolved metal ions, and organic materials [13,14]. From both application and economic point of view for photodecolorization process, the influence of extrinsic factors are considered as important factors to be determined particularly from the optimum decolorization conditions and limitations.

In recent years, artificial neural networks (ANNs) are applied for simulations in different fields of science and engineering. Applying of ANN as the modeling technique is a suitable procedure, due to the intricacy of the reactions in a photocatalytic treatment processes including solving the equations that include the radiant energy balance, the spatial distribution of the absorbed radiation, mass transfer, and mechanisms of these processes [15].

It is known that ANN model can be applied to solve environmental engineering problems. For example, Moral et al. applied the ANN technique for Modeling of DOC Removal from Antibiotics Aqueous Solution by Fenton Process Treatment [16]. Prakash et al. applied ANN to predict the physiochemical wastewater treatment [17]. Frontisti et al. employed ANN for modeling of the photodecolorization of 17a-ethynylestradiol (EE2) in various process conditions using TiO_2-P25 nanoparticles and calculated the relative significance of the operational parameters on the value of 17a-ethynylestradiol photocatalytic decolorization [18]. Ayodele et al. employed ANN to investigate the hierarchy of importance of process variables influencing the degradation of amoxicillin in a heterogeneous photo-Fenton process [19]. However, there are few studies on applications of ANN model in AOPs.

The aim of this research work is to investigate the influence of various parameters on the photocatalytic decolorization of two textile dyes, namely methyl orange (MO) and methylene blue (MB), by UV-light irradiation in the presence of Sn/Zn-TiO_2 nanoparticles. The effects of some operational parameters (such as photocatalyst dosage, initial pollutant concentration, temperature of solution, and reaction time) on the photocatalytic decolorization of MO and MB were investigated and modeled using a multilayer feed-forward neural network model. Also, the relative importance of each operational parameter was calculated based on the connection weights of the ANN model.

2. Experimental

2.1. Materials

MB and MO were two pollutants studied in these experiments which were purchased from Merck and used without any further purification.

In our previous work, we reported preparation of Sn/Zn-TiO_2 nanoparticles from tetrabutyl titanate [Ti$(OC_4H_9)_4$, TBOT], ethanol, and water by sol–gel method [20]. Initially, 5 ml TBOT was slowly dissolved in 15 ml ethanol. Then, a mixture of 5 ml distilled H_2O and 10 ml ethanol was added dropwise into the above mixture. After continuous stirring for 3 h at room temperature, the yellowish transparent sol was obtained. The sol was allowed to stand for 24 h at room temperature and TiO_2 xerogel was obtained. Finally TiO_2 xerogel was calcined in air at 450 °C for 3 h and TiO_2 nanoparticles were obtained [21]. Sn/Zn-TiO_2 (0.75 mol.% Sn, 0.75 mol.% Zn) nanoparticles with a total metal doping of 1.5 mol.% were prepared by the above method, except that the water used for the preparation contained the required amount of $SnCl_4$ and $ZnCl_2$ [10]. Table 1 shows the percentage weight as well as percentage of atomic elements in the sample which resulted from energy dispersive X-ray spectroscopy (EDX) data.

Sn/Zn-TiO_2 nanoparticles was characterized by means of various analysis methods such as X-ray diffraction (XRD), transmission electron microscopy (TEM), EDX and N_2 adsorption–desorption isotherm, and Brunauer–Emmett–Teller (BET). The prepared sample showed specific surface area of 106.3 $m^2 g^{-1}$,

Table 1
Composition (0.75 mol.% Sn, 0.75 mol.% Zn) of Sn/Zn-TiO_2 nanoparticles

Element	Weight (%)	Atomic (%)
Ti	60.15	35.878
O	34.95	62.622
Sn	3.165	0.75
Zn	1.735	0.75

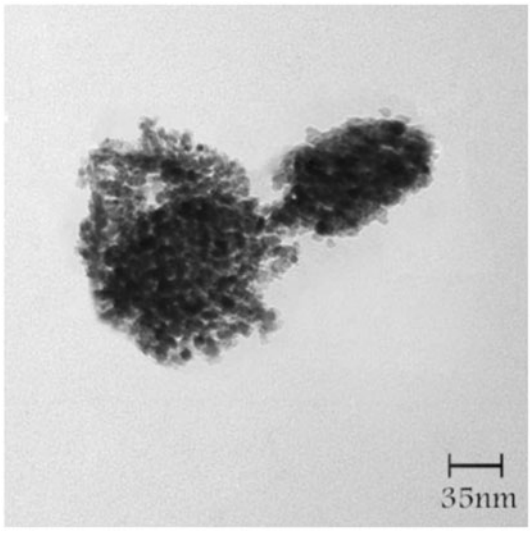

Fig. 1. TEM image of Sn/Zn-TiO_2 nanoparticles.

mean pores diameter of 8.3 nm, and crystallite size of 8–10 nm [20]. The TEM image of the prepared Sn/Zn-TiO_2 nanoparticles is shown in Fig. 1.

2.2. Studies and analysis

Photocatalytic decolorization studies were carried out at atmospheric pressure in a batch quartz reactor, as previously reported [20]. The light was provided by 15 W (UV-C) mercury lamp (with a wavelength peak at 254 nm), which was put above the batch photoreactor. In each run, desired amounts of Sn/Zn-TiO_2 nanoparticles and dyes were fed into the quartz tube reactor and placed in the darkness for 30 min in order to establish an adsorption–desorption equilibrium. The zero time reading was obtained from blank solution kept in the darkness. While vigorous stirring, the reaction mixture was illuminated by UV lamp. Then at certain reaction intervals, 5 ml of sample was withdrawn, centrifuged for 15 min at 5,000 rpm and the concentration of dyes was determined by UV-vis Perkin-Elmer 550 SE spectrophotometer at wavelengths of 665 nm (MB) and 465 nm (MO). Scheme 1 shows chemical structures of MB and MO.

3. Results and discussion

3.1. Effect of the amount of Sn/Zn-TiO_2 photocatalyst on photodecolorization of MB and MO dyes

Fig. 2 shows the effect of the amounts of Sn/Zn-TiO_2 nanoparticles on photodecolorization of MB and MO which investigated under predetermined experimental conditions with MB concentration of 35 mg L^{-1}, MO concentration of 10 mg L^{-1}, reaction time equal to 9 min at room temperature, and changing the weight of Sn/Zn-TiO_2 in range 0.1–0.6 g L^{-1}. It was observed that percentage decolorization of MB was increased from 51.6 to 93.7% in MB and from 46.4 to 88.1% in MO when Sn/Zn-TiO_2 amount was raised from 0.1 to 0.4 g L^{-1}. This increase in the efficiency was due to an increase in the number of active sites on Sn/Zn-TiO_2 surface that in turn increases the rate of $^{\bullet}OH$ and $^{\bullet}O_2$ formation. Further increase in the catalyst amount beyond 0.4 g L^{-1}, the rate of decolorization slightly decreased for both dyes. This reduction in the efficiency was due to the decline in the penetration of UV light with surplus amount of Sn/Zn-TiO_2 nanoparticles [22]. The solution becomes more turbid with the surplus addition of Sn/Zn-TiO_2 nanoparticles and light penetration was deferment [23]. Also, activated molecules could be deactivated due to collision by ground state molecules in the result of the addition of surplus Sn/Zn-TiO_2 nanoparticles [24]. An amount of 0.4 g L^{-1} of photocatalyst was used for the subsequent photocatalytic decolorization experiments.

The results showed that photodecolorization rate of MB is much higher than MO. The required irradiation time for 35 mg L^{-1} MB is equal to the required irradiation time for 10 mg L^{-1} MO. It is concluded that photocatalytic decolorization rate of dyes is affected by the chemical structure of dyes. It is well known that under illumination of Sn/Zn-TiO_2 by UV light, electron–hole pairs are generated. As shown in Scheme 1, MO is an azo dye and MB is a thiazine dye. The existence of a positively charged N^+ group in MB molecular structure causes to interact it by the excited electrons of the photocatalyst Sn/Zn-TiO_2 leads to the fast oxidation of MB through holes, whereas the presence of a withdrawing group, SO_3^-, is probably at the origin of the less efficient of MO decolorizations. The low decolorization rate of MO as an azo dye is due to difficult conversion of N atoms in the structure of MO into oxidized nitrogen compounds. The interaction of aliphatic chain with $^{\bullet}OH$ is small and these radicals are short lived [25]. However the decolorization of MO solution is related to cleavage of the azo linkage in MO molecules. The nitrogen to nitrogen double bonds (–N=N–) as characteristic of azo dyes are the most active bonds in azo dye molecules and determine their olors. These bonds can be oxidized either by positive holes or $^{\bullet}OH$ [26].

3.2. Effect of initial dye concentration

The effect of change in initial dye concentration on decolorization percentage in range (10–70 mg L^{-1}) was investigated by keeping other experimental conditions

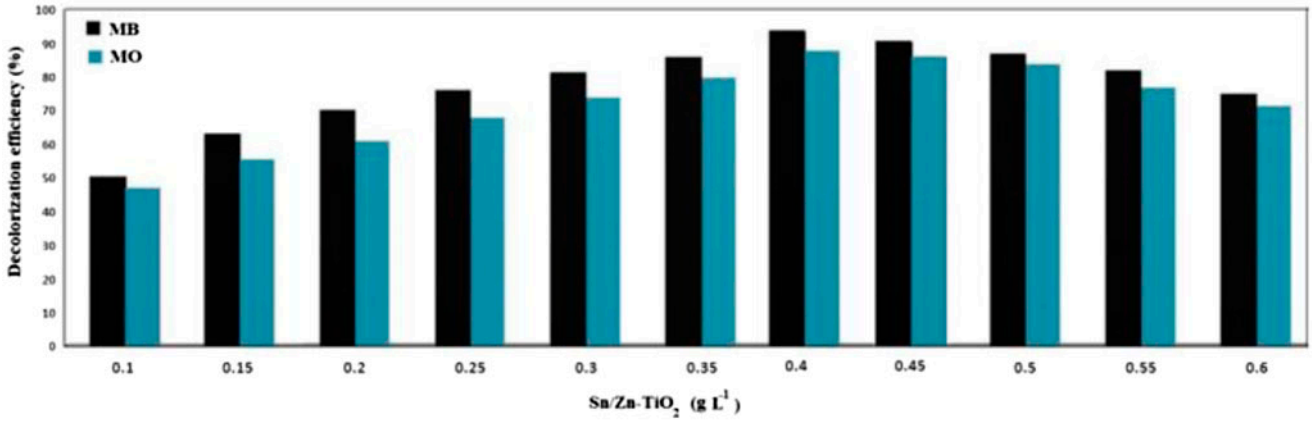

Fig. 2. Effect of Sn/Zn-TiO_2 dosage on the decolorization efficiency of MB and MO. $[MB]_0 = 35\ mg\ L^{-1}$, $[MO]_0 = 10\ mg\ L^{-1}$, $t = 9$ min, and temperature of solution = 298 K.

constant at room temperature, reaction time equal to 9 min, and 0.4 g L^{-1} catalyst concentration. It can be seen from Fig. 3 that the decolorization efficiency decreases as the initial dyes concentration increases. This behavior can be explained by following reason:

- With increasing of the dye concentration, more and more organic substances and intermediates are adsorbed on the surface of photocatalyst, and therefore the reaction of dye molecules with photogenerated holes or hydroxyl radicals is inhibited due to the lack of any direct contact between them [27,28].
- At high concentration of dye, the photocatalyst surface was covered mainly by pollutant molecules and production of $^{\bullet}OH$ and $^{\bullet}O_2^-$ superoxide radicals were decreased [29].

3.3. Effect of reaction time

The effect of UV-light irradiation time on the photocatalytic decolorization of MB and MO was investigated from 2 to 17 min, at 35 mg L^{-1} MB concentration, 10 mg L^{-1} MO concentration, 0.4 g L^{-1} catalyst concentration, and at room temperature. The results are shown in Fig. 4. The results clearly show that the photodecolorization efficiency increases with time. After 9 min, the percentage of decolorization is not changed so much.

3.4. Effect of temperature

The effect of change in reaction temperature on decolorization percentage in range (293–313 K) was investigated by keeping other experimental conditions

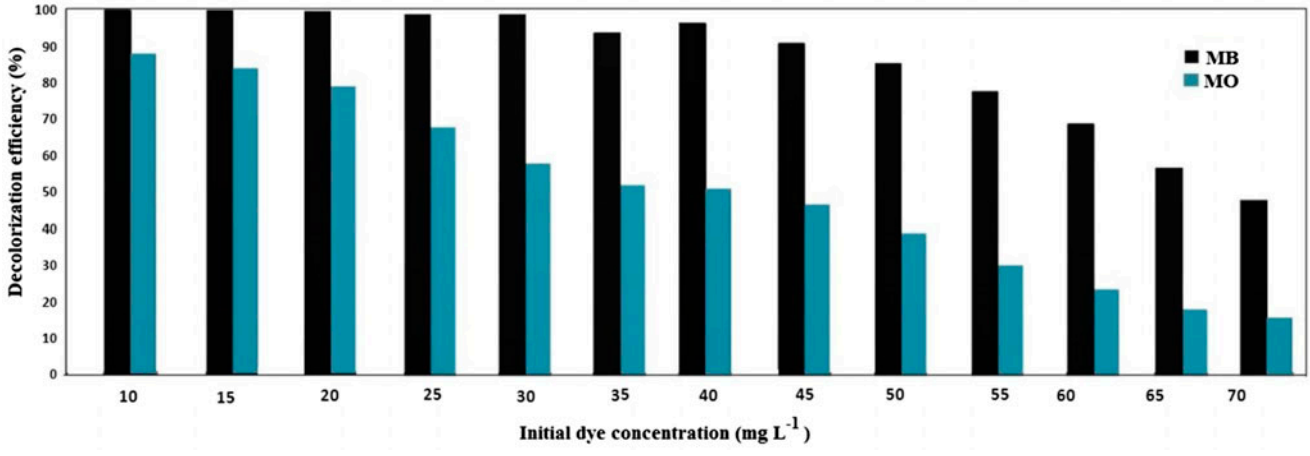

Fig. 3. Effect of initial dyes concentration on the decolorization efficiency of MB and MO. $[Sn/Zn\text{-}TiO_2]_0 = 0.4\ g\ L^{-1}$, $t = 9$ min, and temperature of solution = 298 K.

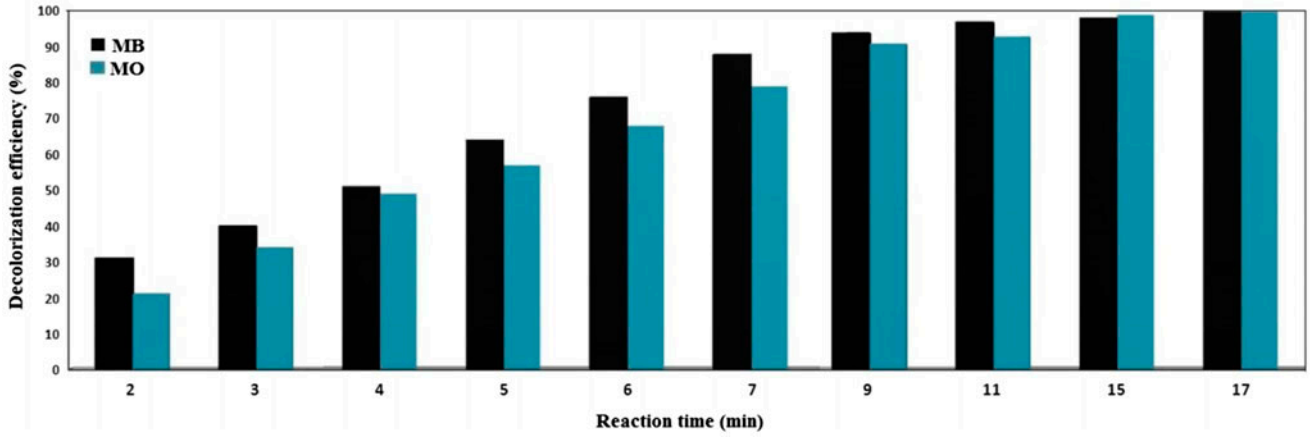

Fig. 4. Effect of reaction time on the decolorization efficiency of MB and MO. $[Sn/Zn\text{-}TiO_2]_0 = 0.4\ g\ L^{-1}$, $[MB]_0 = 35\ mg\ L^{-1}$, $[MO]_0 = 10\ mg\ L^{-1}$, and temperature of solution = 298 K.

constant at MO concentration of 10 mg L^{-1}, MB concentration of 35 mg L^{-1}, reaction time equal to 9 min, and Sn/Zn-TiO_2 catalyst dosage of 0.4 g L^{-1}. The results are plotted in Fig. 5. It can be seen that decolorization rate of MB increased from 90.11 to 99.05% in MB and from 89.2 to 95.14% in MO when the temperature was increased from 293 to 313 K for both dyes. Therefore, the photocatalytic reaction is not very temperature dependent. It is well known that electron–hole pair generation in the presence of light source is responsible for initiation of photoreaction. Therefore, the photodecolorization systems are usually operated at room temperature and do not need heating.

3.5. ANN modeling

ANNs is a well-known method for its ability in learning, simulation, and prediction of experimental data. A multilayered perceptron neural net has an input layer of neuron (independent variables), a number of hidden layers, and the output layer (dependent variables). The number of input and output neurons is

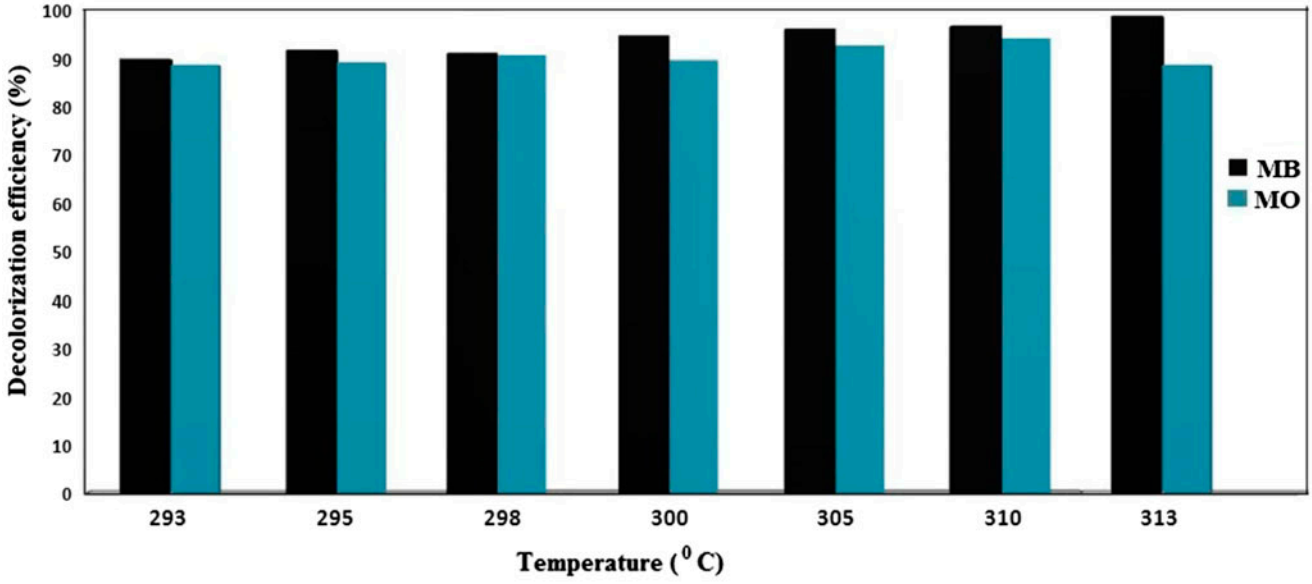

Fig. 5. Effect of temperature of solution on the decolorization efficiency of MB and MO. $[Sn/Zn\text{-}TiO_2]_0 = 0.4\ g\ L^{-1}$, $[MB]_0 = 35\ mg\ L^{-1}$, $[MO]_0 = 10\ mg\ L^{-1}$, and $t = 9$ min.

Table 2
The ranges of input and output variables

Variable	Range of the parameter value
Input layer	
$Sn/Zn\text{-}TiO_2$ dosage ($g\,L^{-1}$)	0.1–0.6
Initial dye concentration ($mg\,L^{-1}$)	15–70
Reaction time (min)	2–17
Temperature (K)	293–313
Output layer	
Decolorization efficiency (%)	31–99.9 (for MB) 14–100 (for MO)

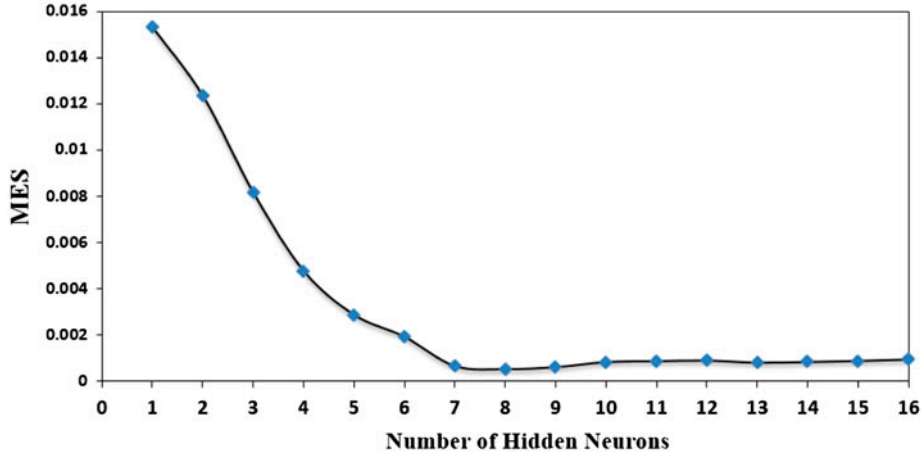

Fig. 6. Effect of the number of neurons in the hidden layer on the performance of the neural network.

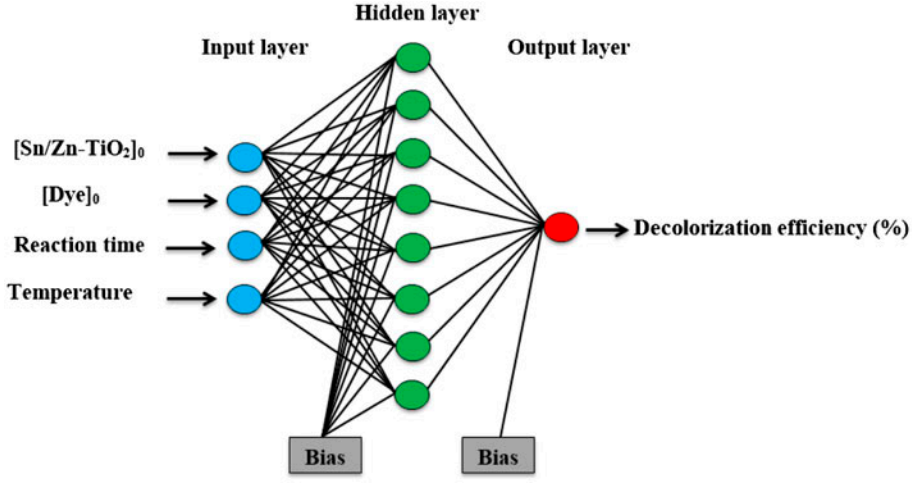

Fig. 7. Schematic illustration of the optimized ANN structure.

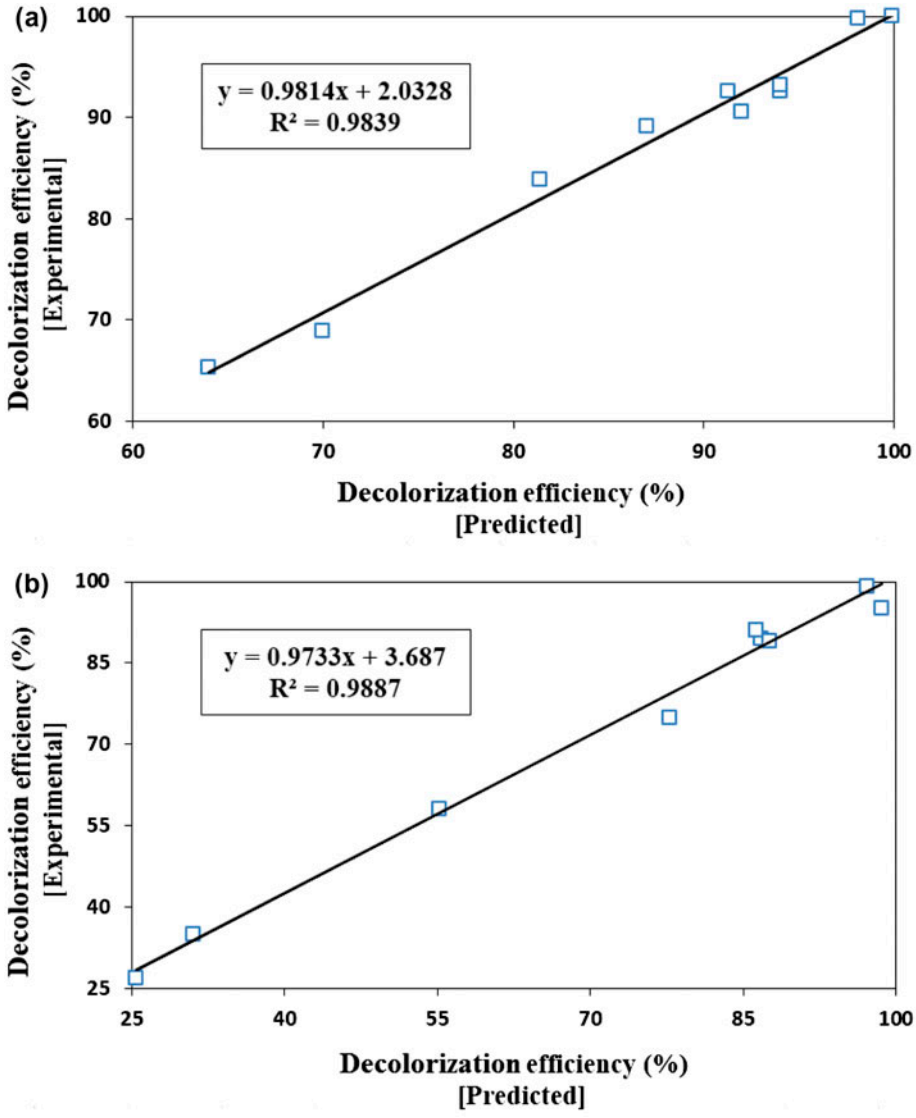

Fig. 8. Comparison between ANN predicted and experimental decolorization efficiency (%) values for the test set of (a) MB and (b) MO dyes decolorization.

determined by the nature of the problem. The hidden layers act like feature detectors; there can be more than one hidden layer. In this study, Matlab mathematical software, 2011a version, was used for ANN calculations. Moreover, a three-layered back-propagation algorithm with tangent sigmoid transfer function (tansig) at hidden layer, and a linear transfer function (purelin) at output layer were designed.

3.6. Modeling of operational variables

The input operational variables of the network were the Sn/Zn-TiO_2 dosage, initial dye concentration, reaction time, and temperature, and the corresponding decolorization efficiency (%) was used as an output of the network. The ranges of operational parameters are given in Table 2.

The ANN model used experimental data-sets in different conditions to test training. The experimental data-sets were split into training (1/2), validation (1/4) and test (1/4) subsets. All inputs and target data must be scaled within a specified range. Therefore, all data (X_i) were scaled (x_i) into the 0.2–0.8 ranges, through Eq. (1) [30];

$$x_i = 0.2 + \frac{0.6\,(X_i - X_{\min})}{X_{\max} - X_{\min}} \quad (1)$$

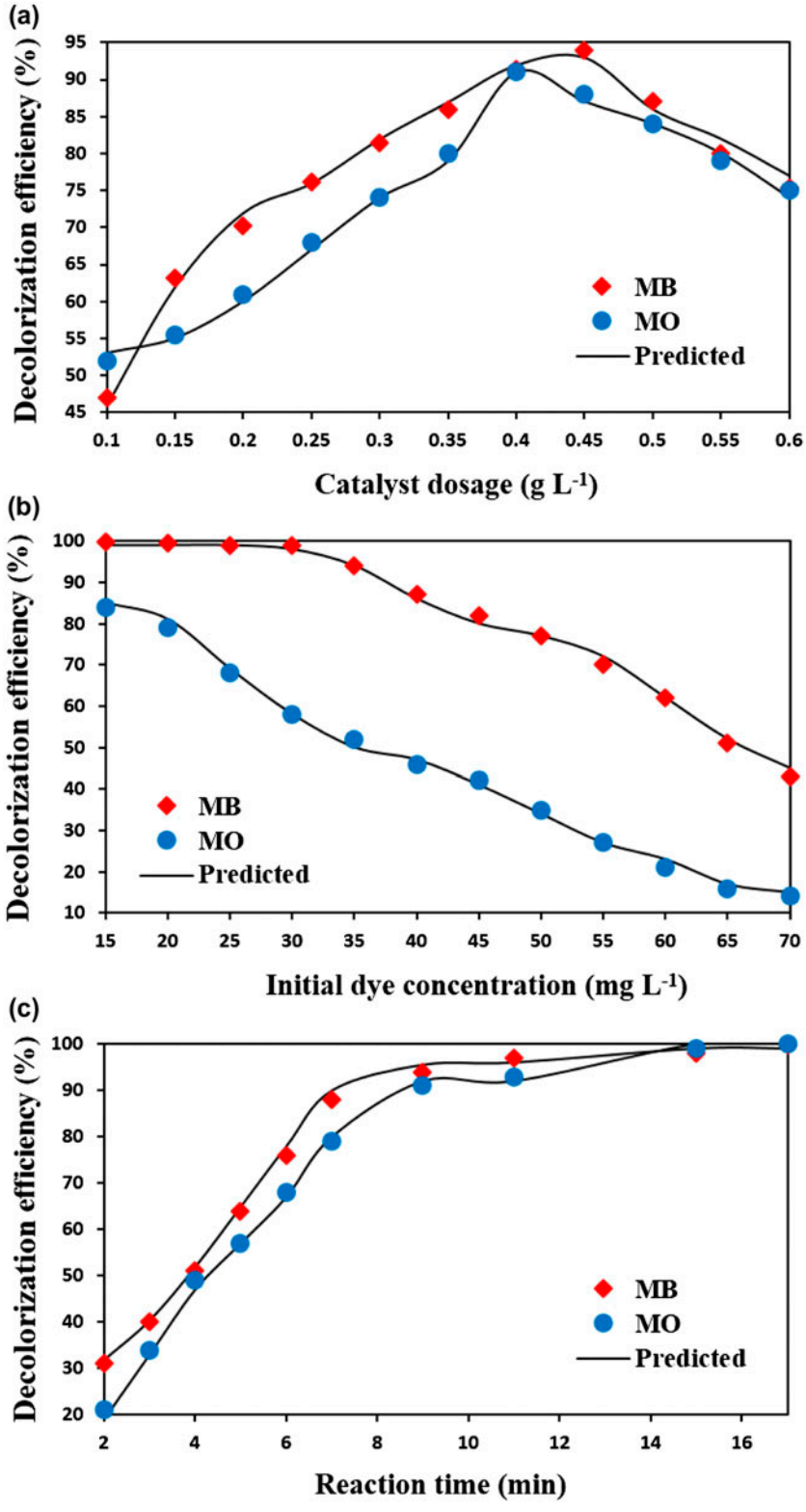

Fig. 9. Comparison between ANN predicted and experimental values of MB and MO decolorization efficiency (%) as a function of operational variables: (a) catalyst dosage, (b) initial dye concentration, (c) reaction time, and (d) temperature.

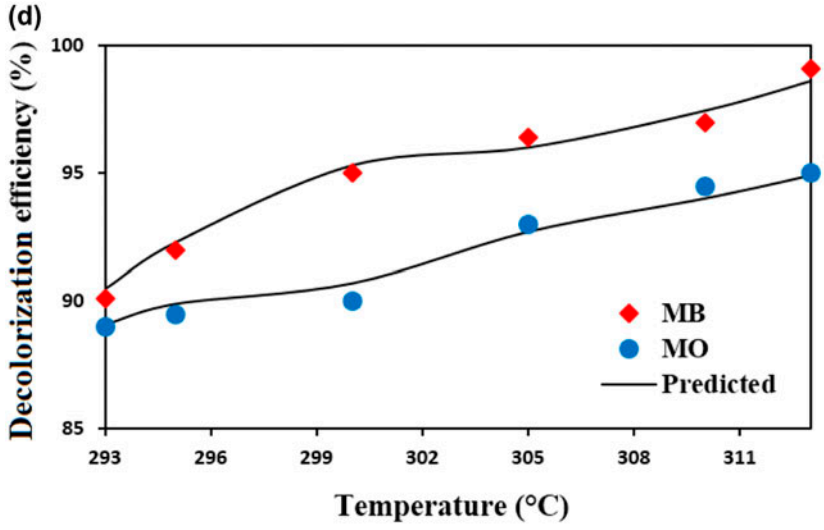

Fig. 9. (*Continued*)

Table 3
Weight matrix for decolorization of MB dye: weight between input and hidden layers (W_1) and weights between hidden and output layers (W_2)

W_1 Input variable						W_2 Output	
Neuron	Sn/Zn-TiO_2 dosage	Initial MB concentration	Reaction time	Temperature	Bias	Neuron	Decolorization efficiency (%)
1	−2.242	−0.391	0.216	0.561	2.3534	1	0.282
2	−0.652	0.134	−1.417	−1.267	−2.422	2	0.9069
3	1.0984	1.108	−1.3	−1.106	−0.87	3	−0.619
4	0.4838	−1.692	−1.604	−0.633	0.0857	4	1.0474
5	2.2505	0.784	0.808	0.545	−0.258	5	−1.268
6	0.7263	1.715	−0.227	1.389	0.9056	6	0.2462
7	0.1748	0.027	−1.414	1.638	1.9446	7	1.0727
8	1.3965	1.73	−0.074	−0.679	2.3724	8	−0.506
						Bias	0.1255

where X_{min} and X_{max} refer to the lowest and the highest value of the input variable X_i, respectively.

The number of neurons in the hidden layer affects the performance of the ANN model. To determine the optimum number of hidden nodes in this study, different numbers of neurons were tested in the range of 1–16, in the hidden layer. Each topology was repeated three times to avoid random correlation due to random initialization of weights. Fig. 6 shows the relationship between the mean square error (MSE) and the number of neurons in the hidden layer. As it can be seen, the lowest MSE is obtained in about eight neurons; therefore, eight neurons were selected for the best performance of neural network model. Fig. 7 shows the schematic illustration of the optimized ANN structure.

Fig. 8 shows a comparison between experimental and predicted decolorization efficiency (%) values for the test set by using neural network model. The plots in these figures have correlation coefficient (R^2) of 0.9839 and 0.9887, respectively, for MB and MO dyes. From this plots, it can be seen that the results obtained from the models are in good agreement with the experimental data, and the model can accurately predict decolorization efficiency of both MB and MO dyes under different conditions.

Table 4
Weight matrix for decolorization of MO dye: weight between input and hidden layers (W_1) and weights between hidden and output layers (W_2)

W_1 Input variable						W_2 Output	
Neuron	Sn/Zn-TiO_2 dosage	Initial MO concentration	Reaction time	Temperature	Bias	Neuron	Decolorization efficiency (%)
1	0.6477	−0.775	2.097	−0.343	2.3577	1	−0.048
2	−0.4	−1.184	1.034	−1.36	2.0052	2	0.3215
3	−1.448	0.789	0.285	1.747	−0.729	3	−0.265
4	−1.789	−1.032	−0.943	0.613	−0.355	4	0.6447
5	−0.389	−1.32	1.905	−0.243	−0.137	5	0.7305
6	−0.888	0.751	−0.858	1.976	0.9176	6	0.933
7	0.9963	−0.637	1.72	−1.024	−1.711	7	0.4353
8	−0.809	1.001	−1.727	0.951	2.3528	8	−0.113
						Bias	0.345

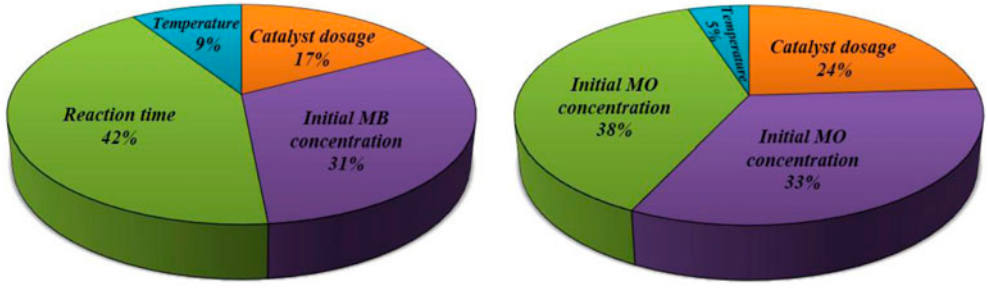

Fig. 10. Relative importance (%) of the input (a) synthesis and (b) operational variables on the decolorization efficiency (%) values.

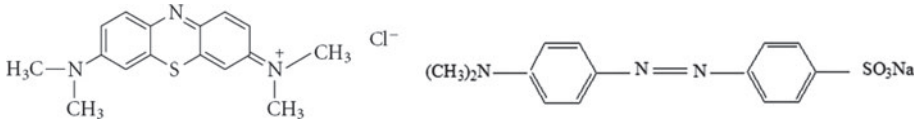

Scheme 1. Chemical structures of MB and MO.

Fig. 9 shows a comparison between the predicted values from ANN model and experimental results of the output variable (removal efficiency (%)) as a function of operational variables. These results confirm that the designed ANN model provides a reliable method to predict adequately the photocatalytic decolorization efficiency of both MB and MO dyes under different conditions, since agreement between the values predicted by the ANN model and the experimental results is good.

3.7. ANN model sensitivity analysis

Tables 3 and 4 show the weights produced by the ANN models used in this study for decolorization of both MB and MO dyes, respectively. The relative importance of the influence of each input variable on output variable can be obtained through the neural weight matrix [31].

For every input variable, the percentage change in the output, as a result of the change in the input variable, was calculated using the following Eq. (2) [32]:

$$I_j = \frac{\sum_{m=1}^{m=N_h} ((|W_{jm}^{ih}|/\sum_{k=1}^{N_i} |W_{km}^{ih}|) \times |W_{mn}^{ho}|)}{\sum_{k=1}^{k=N_i} \{\sum_{m=1}^{m=N_h} (|W_{km}^{ih}|/\sum_{k=1}^{N_i} |W_{km}^{ih}|) \times W_{mn}^{ho}\}} \quad (2)$$

where I_j is the relative importance of the jth input variable on the output variable, N_i and N_h are the number of inputs and hidden neurons, respectively; W's are connection weights, the superscripts "i", "h", and "o", respectively, refer to input, hidden, and output layers; and subscripts "k", "m", and "n", respectively, refer to input, hidden, and output neurons.

Fig. 10 represents a comparison between the relative importance of input variables as calculated by Eq. (2) on the decolorization efficiency of MB and MO dyes. As Fig. 10 indicates, for both dyes, reaction time has greater effect on the photocatalytic decolorization of dyes, followed by initial dye concentration and catalyst dosage, while the solution temperature was determined as the parameter with weak influence on the decolorization efficiency of both dyes.

4. Conclusions

The photocatalytic decolorization of two textile dyes mediated by Sn/Zn-TiO_2 nanoparticles was successfully achieved. Results showed that the photocatalytic activity of Sn/Zn-TiO_2 nanoparticles synthesized via sol–gel method is highly depending on the photocatalyst dosage, initial concentration of dye, UV-irradiation time, and solution temperature. Also, the effect of these operational parameters on the photocatalytic decolorization of MB and MO was modeled by the ANN technique. A three-layered back-propagation neural network with tangent sigmoid transfer function (tansig), at the hidden layer with eight neurons, was designed to predict the removal of MB and MO under different operational conditions. The performance of synthesized Sn/Zn-TiO_2 nanoparticles in the dyes decolorization was successfully simulated by using neural network modeling, and a good agreement was obtained between the predicted results from the ANN model and the experimental results, with a correlation coefficient (R^2) of 0.9839 and 0.9887 for MB and MO dyes, respectively. The sensitivity analysis showed that the reaction time has a larger effect on the photocatalytic decolorization of dyes, whereas the temperature of solution has the lowest effect on the photocatalytic decolorization of dyes.

Acknowledgment

We thank the Payame Noor University I.R. of Iran for supporting this research.

References

[1] A.R. Khataee, M.B. Kasiri, Photocatalytic degradation of organic dyes in the presence of nanostructured titanium dioxide: Influence of the chemical structure of dyes, J. Mol. Catal. A: Chem. 328 (2010) 8–26.
[2] H.R. Ebrahimi, M. Modrek, M. Mozaffari, Photo decolorization of direct red 81 (5-solamine) by using zinc oxide nanoparticles on glass granule substrate in acidic pH and various atmospheres, World. Appl. Sci. J. 19 (2012) 352–354.
[3] T. Robinson, G. McMullan, R. Marchant, P. Nigam, Remediation of dyes in textile effluent: A critical review on current treatment technologies with a proposed alternative, Bioresour. Technol. 77 (2001) 247–255.
[4] H. Gopalappa, K. Yogendra, K.M. Mahadevan, Solar photocatalytic decolorization of commercial azo dye acid orange 7 by synthesized $CaZnO_2$ nanoparticle as an effective catalyst, Int. J. Res. Chem. Environ. 2 (2012) 39–43.
[5] S. Ledakowicz, M. Solecka, R. Zylla, Biodegradation, decolourisation and detoxification of textile wastewater enhanced by advanced oxidation processes, J. Biotechnol. 89 (2001) 175–184.
[6] D. Georgiou, P. Melidis, A. Aivasidis, K. Gimouhopoulos, Degradation of azo-reactive dyes by ultraviolet radiation in the presence of hydrogen peroxide, Dyes Pigm. 52 (2002) 69–78.
[7] V.D. Gosavi, S. Sharma, A general review on various treatment methods for textile wastewater, J. Environ. Sci. Comput. Sci. Eng. Tech. 3 (2014) 29–39.
[8] H. Nagpure, V. Banakar, R. Dhanda, K.S. Wani, Degradation of paper mill wastewater using batch (photo catalytic) reactor, Int. J. Green Chem. Bioprocess. 3 (2013) 24–29.
[9] Y. Xie, C. Yuan, Characterization and photocatalysis of Eu^{3+}–TiO_2 sol in the hydrosol reaction system, Mater. Res. Bull. 39 (2004) 533–543.
[10] R. Mohammadi, B. Massoumi, M. Rabani, Photocatalytic decomposition of amoxicillin trihydrate antibiotic in aqueous solutions under UV irradiation using Sn/TiO_2 nanoparticles, Int. J. Photoenergy 2012 (2012) 1–11, ID 514856.
[11] L. Kumaresan, M. Mahalakshmi, M. Palanichamy, V. Murugesan, Synthesis, characterization, and photocatalytic activity of Sr^{2+} doped TiO_2 nanoplates, Ind. Eng. Chem. Res. 49 (2010) 1480–1485.
[12] T.A. Segne, S.R. Tirukkovalluri, S. Challapalli, Studies on characterization and photocatalytic activities of visible light sensitive TiO_2 nano catalysts co-doped with magnesium and copper, Int. Res. J. Pure Appl. Chem. 1 (2011) 84–103.
[13] J.M. Herrmann, Heterogeneous photocatalysis: Fundamentals and applications to the removal of various types of aqueous pollutants, Catal. Today 53 (1999) 115–129.

[14] I.K. Konstantinou, T.A. Albanis, TiO_2-assisted photocatalytic degradation of azo dyes in aqueous solution: Kinetic and mechanistic investigations, Appl. Catal., B 49 (2004) 1–14.
[15] M. Mohammadian Fazli, A.R. Mesdaghinia, K. Naddafi, S. Nasseri, M. Yunesian, M. Mazaheri Assadi, S. Rezaie, H. Hamzehei, Optimization of reactive blue 19 decolorization by *ganoderma* sp. Using response surface methodology, Iran J. Environ. Health Sci. Eng. 7 (2010) 35–42.
[16] H. Moral, A. Aksoy, C.F. Gokcay, Modeling of the activated sludge process by using artificial neural networks with automated architecture screening, Comput. Chem. Eng. 32 (2008) 2471–2478.
[17] N. Prakash, S.A. Manikandan, L. Govindarajan, V. Vijayagopal, Prediction of biosorption efficiency for the removal of copper(II) using artificial neural networks, J. Hazard. Mater. 152 (2008) 1268–1275.
[18] Z. Frontistis, V.M. Daskalaki, E. Hapeshi, C. Drosou, D. Fatta-Kassinos, Photocatalytic (UV-A/TiO_2) degradation of 17α-ethynylestradiol in environmental matrices: Experimental studies and artificial neural network modeling, J. Photochem. Photobiol., A 240 (2012) 33–41.
[19] O.B. Ayodele, H.S. Auta, N. Nor, Artificial neural networks, optimization and kinetic modeling of amoxicillin degradation in photo-Fenton process using aluminum pillared montmorillonite-supported ferrioxalate catalyst, Ind. Eng. Chem. Res. 51 (2012) 16311–16319.
[20] R. Mohammadi, B. Massoumi, H. Eskandarloo, Preparation and characterization of Sn/Zn/TiO_2 photocatalyst for enhanced amoxicillin trihydrate decolorization, Desalin. Water Treat. 12 (2013) 1–10.
[21] M.A. Behnajady, H. Eskandarloo, N. Modirshahla, M. Shokri, Investigation of the effect of sol–gel synthesis variables on structural and photocatalytic properties of TiO_2 nanoparticles, Desalination 278 (2011) 10–17.
[22] M.S.T. Gonçalves, A.M.F. Oliveira-Campos, E.M.M.S. Pinto, P.M.S. Plasência, M.J.R.P. Queiroz, Photochemical treatment of solutions of azo dyes containing TiO_2, Chemosphere 39 (1999) 781–786.
[23] A. Akyol, H.C. Yatmaz, M. Bayramoglu, Photocatalytic decolorization of Remazol Red RR in aqueous ZnO suspensions, Appl. Catal., B 54 (2004) 19–24.
[24] N. Daneshvar, D. Salari, A.R. Khataee, Photocatalytic degradation of azo dye acid red 14 in water: Investigation of the effect of operational parameters, J. Photochem. Photobiol., A 157 (2003) 111–116.
[25] E.M. Saggioro, A.S. Oliveira, T. Pavesi, C.G. Maia, L.F. Ferreira, J.C. Moreira, Use of titanium dioxide photocatalysis on the remediation of model textile wastewaters containing azo dyes, Molecules. 16 (2011) 10370–10386.
[26] M. Karkmaz, E. Puzenat, C. Guillard, J.M. Herrmann, Photocatalytic degradation of the alimentary azo dye Amaranth, Appl. Catal., B 51 (2004) 183–194.
[27] T.K. Tan, P.S. Khiew, W.S. Chiu, S. Radiman, R. Abd-Shukor, N.M. Huang, H.N. Lim, Photodegradation of phenol red in the presence of ZnO nanoparticles, World Acad. Sci. Eng. Technol. 5 (2011) 7–21.
[28] K. Selvam, M. Muruganandham, I. Muthuvel, M. Swaminathan, The influence of inorganic oxidants and metal ions on semiconductor sensitized photodegradation of 4-fluorophenol, Chem. Eng. J. 128 (2007) 51–57.
[29] S. Munesh, R.C. Meena, Photocatalytic decolorization of acid red 186 using alternative developed photocatalyst MBIR Dowex 11, Res. J. Chem. Sci. 2 (2012) 56–62.
[30] M.B. Kasiri, H. Aleboyeh, A. Aleboyeh, Modeling and optimization of heterogeneous photo-Fenton process with response surface methodology and artificial neural networks, Environ. Sci. Technol. 42 (2008) 7970–7975.
[31] G.D. Garson, Interpreting neural-network connection weights, AI Expert 6 (1991) 47–51.
[32] A. Aleboyeh, M.B. Kasiri, M.E. Olya, H. Aleboyeh, Prediction of azo dye decolorization by UV/H_2O_2 using artificial neural networks, Dyes Pigm. 77 (2008) 288–294.